Recent Advances in Understanding Flow Effects on Polymer Crystallization

Julia A. Kornfield,*,† Guruswamy Kumaraswamy,‡ and Ani M. Issaian†

Division of Chemistry and Chemical Engineering, California Institute of Technology, Pasadena, California 91125, and Division of Polymer Chemistry, National Chemical Laboratory, Pune 411008, India

Molecular aspects of polymer melt rheology play an extremely strong role in governing the processing−structure−property relations of semicrystalline polymers, the dominant materials in the plastics industry. Recent advances in experimental apparatus and methods have revealed that the dramatic changes in crystallization kinetics and morphology induced during shear follow a kinetic pathway. The rate of formation of oriented precursors is not limited by the usual activation barrier to nucleation but instead occurs many orders of magnitude faster, at a rate that tracks the dynamics of the polymer chains in the melt. Model polymers and their binary blends have shown that the relevant melt dynamics that control formation of the oriented threadlike nuclei are those of the longest chains in the melt and that the effect of the long chains is cooperative, greatly enhanced by long chain−long chain overlap. Thus, insights gained into the role of chain dynamics in the molecular mechanism of shear-enhanced crystallization may soon combine with parallel advances over the past decade regarding the dynamics of polydisperse melts to provide the underpinnings for truly predictive models of flow-enhanced crystallization of polymers.

Introduction

Semicrystalline polymers comprise over two-thirds of the annual production of all synthetic polymers and find use in applications that range from carpet fibers to car fascia, including biomedical applications such as sutures and hip implants, and a diversity of applications in personal electronics such as insulators, connectors, and housing materials.[1] A crystalline−amorphous composite structure spontaneously forms as these polymers crystallize during processing, resulting in a material that derives strength from the crystallites and toughness from the noncrystalline material between them. Semicrystalline polymers are highly versatile because of their tunability: altering the processing conditions changes the spatial organization and alignment of crystallites[2] and thus influences material properties such as strength, hardness, permeability, surface texture, transparency—almost every functional property that is of interest for this classic material. Because of the profound role of rheology and the vast engineering significance of the problem, we are pleased to contribute a paper on shear-induced crystallization to the special issue honoring the career of Bill Schowalter.

The morphology of "semicrystalline" polymers is unlike that of small-molecule or atomic crystals. In polymers, crystallization is never complete because the chainlike nature of the molecule hinders equilibrium, "complete" crystallization.[3] Thus, a kinetically determined, nonequilibrium structure is formed, comprising ordered crystalline and disordered amorphous regions that coexist in apparent violation of the Gibbs phase rule.[3] The connectivity of polymer molecules also has consequences for their flow behavior:[4] polymers exhibit stress relaxation times that are orders of magnitude higher than for common Newtonian liquids, so that typical processing flows significantly distort chain conformation, and the stress can be *directly* related to the anisotropy in polymer chain configuration.[4]

When polymers crystallize from melts subject to flow, the semicrystalline morphology that develops is controlled by the interplay between crystallization and chain relaxation.[5] Crystallization kinetics can be accelerated by orders of magnitude, and dramatic changes in morphology can be induced. Processing operations typically involve some combination of fairly intense shear and extensional flow, so it is of considerable importance to understand how processing influences microstructure formation in semicrystalline polymers. The goal of our work is to discover the molecular level processes that control structure formation in semicrystalline polymers under the flow conditions that are typically imposed during processing.

There is a vast body of literature that describes the effects of flow on polymer crystallization, which has been summarized previously.[6,7] The majority of these studies can be categorized as (i) experiments that are performed in processing equipment[8] to examine crystallization during a particular processing operation (such as molding or fiber spinning, etc.) or (ii) experiments performed under "controlled" thermal and flow conditions[9] in a laboratory rheometer. The primary limitation of the former experiments is that the complicated thermal and flow history experienced by the crystallizing polymer make it difficult to separate out the effects of flow from those of thermal gradients and transients. In addition, materials available in large enough quantities for these studies have generally been ill defined, precluding molecular-level interpretation of the results. In the latter rheometer experiments, the typical combination

* To whom correspondence should be addressed. Tel: 1-626-395-4138. Fax: 1-626-568-8743. E-mail: jak@cheme.caltech.edu.
† California Institute of Technology.
‡ National Chemical Laboratory.

10.1021/ie020237z CCC: $22.00 © 2002 American Chemical Society
Published on Web 10/19/2002

of stress, strain, and strain rate that characterize processing operations cannot be attained. Due to the highly nonlinear character of the effects of flow on crystallization, it is not possible to generalize the results to the high levels of stress and strain typically imposed in polymer processing. Despite the limitations of both of these types of experiments, some features of flow-enhanced crystallization are widely accepted: the kinetics of crystallization is greatly accelerated by flow, and flow can induce the formation of anisotropic crystallites, oriented in the flow direction. However, a deeper understanding of flow effects on polymer crystallization has been frustrated by the difficulties involved in designing experiments to follow the rapid processes of crystal nucleation and growth under intense flow conditions, and predictive models remain elusive despite decades of research.

About a decade ago, the group of Janeschitz-Kriegl designed an experiment (called "short-term" shearing[10]) that was radically different from their predecessors. In their elegant approach, the high stresses characteristic of processing are combined with well-defined thermal and flow conditions (isothermal crystallization following a brief interval of shear). This experimental protocol allowed them to isolate the effect of flow from thermal transients or temperature gradients and to systematically probe the effects of the shear stress and duration.

Recently, we constructed an apparatus to extend the short-term shearing approach to well-defined polymers with comprehensive characterization of the real-time development of structure and the final solid-state morphology.[6] Our design allows us to work with small amounts of sample (total loading of 5−10 g, with each experiment requiring less than 0.5 g) compared to the roughly 20 kg of sample required to operate the extruder-fed instrument.[10] This ability to work with small amounts of sample opens up studies of model polymers that might be available only in several-gram quantities. Further, our design allows an arsenal of optical and X-ray probes to track microstructural development in situ and enables facile removal of the sample for ex situ microscopy.

We have investigated shear-enhanced crystallization of isotactic polypropylene[11−14] using a combination of in situ rheo-optical and rheo-synchrotron scattering and ex situ optical and transmission electron microscopy (TEM). In this paper, we review our recent work,[11−14] highlighting some of the surprising results of our studies and discussing their implications for our understanding of the effects of flow on polymer crystallization. In brief, we have shown that flow can open a kinetic pathway to nucleation, such that the rate of nucleation tracks the rate of molecular motion in the melt. Oriented precursors formed during flow template subsequent oriented growth; the distance between the precursors governs the time for completion of the oriented structure. Formation of the oriented precursors is greatly enhanced by having a distribution of chain lengths that includes a small amount of chains that are much longer than average, a "high molecular weight tail". Model materials allow us to be specific about the length and amount of long chains, leading to the finding that the long chains do not act alone but instead act cooperatively in a way that benefits greatly from overlap among the long chains. Each of these new advances points the way to future theoretical work and improved models for predicting the processing behavior of the dominant class of synthetic polymers, the semicrystalline polymers.

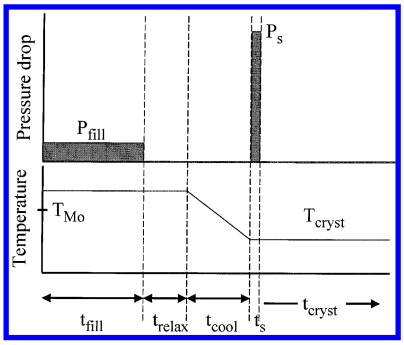

Figure 1. Experimental protocol for shear-enhanced crystallization experiments. The polymer melt is extruded from the reservoir using a low-pressure drop P_{fill} for a time t_{fill} (top graph); then it is allowed to relax for time t_{relax} at a temperature that is above the equilibrium melting temperature, T_{Mo} (bottom graph). When the polymer melt has relaxed, it is cooled to the crystallization temperature, T_{cryst}, and then subjected to shear by imposing a high-pressure drop, P_s, for a brief interval, t_s.

Experimental Section

Features of the Shear Apparatus. The short-term shearing protocol designed by Janeschitz-Kriegl generates well-defined initial conditions for the crystallization experiment and imposes a controlled and simple stress profile (Figure 1). The original experiments were implemented as follows.[10] Polymer held in a reservoir is injected into a slit die. The die is held at a high temperature to erase the memory of the filling process (t_{relax}) and then cooled (t_{cool}) to the desired crystallization temperature (T_{cryst}), which is selected such that the quiescent crystallization time is much longer than the shearing time. Thus, any oriented crystallites that are observed arise because of early events during shear (during the short shearing time t_s), not obscured by deformation-induced reorientation of crystallites after they have formed. Once a fully isothermal, subcooled condition is reached, the polymer melt is subjected to intense shearing at wall shear stresses similar to those in polymer processing for a brief shearing time (t_s). The polymer subsequently crystallizes, and the progress of crystallization is monitored using a variety of structural probes. The apparatus is relatively compact and can be transported to a synchrotron source for real-time X-ray scattering measurements. Thus, in situ structure development can be monitored using turbidity, birefringence, and dichroism with visible and IR radiation (characteristic of the appearance of crystallites and the orientation of molten chains and crystallites), wide-angle X-ray diffraction (WAXD; characteristic of unit cell structures and orientation), and small-angle X-ray scattering (SAXS; characteristic of nanoscale lamellar structures).

The implementation of this protocol requires the ability (i) to generate a brief, intense flow that can be started and stopped rapidly and (ii) to cool to T_{cryst} without significant undershoot and then keep the temperature stable. We use a pneumatic actuator controlled by a high-speed solenoid-activated valve to generate sharp shear "pulses" (rise and fall times $\sim$ 50 ms), with control over the pulse duration (from 250 ms to over 10 s) and the pressure drop to drive polymer through a slit die (Figure 2). The pressure recorded at the entrance of the flow channel is used to compute the wall shear

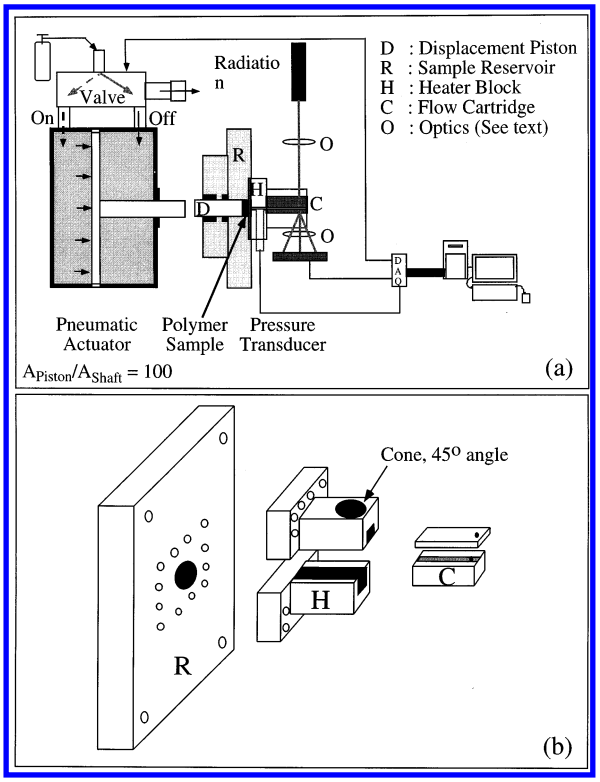

Figure 2. (a) Schematic diagram of the shear instrument. (b) Isometric view of the reservoir (R), heater block (H), and cartridge (C) indicating how they fit together: H bolts onto R, and C slides into H and is held in place by a plate that bolts onto the face of H. The perspective shown in part b is upside down relative to part a: light exits through the conical aperture to permit light and X-ray scattering measurements. Reprinted with permission from ref 6. Copyright 1999 American Institute of Physics.

stress σ_w from a macroscopic force balance. Pressures up to 70 MPa are generated in the reservoir (corresponding to $\sigma_w \approx 0.1$ MPa). This stress level approaches that encountered in industrial processes, which typically operate near the limit imposed by the onset of flow instabilities beyond this value of wall shear stress.[15] The flow cartridge (C) fits snugly in a thermal reservoir (H), whose temperature is controlled using a combination of cartridge heaters with proportional−integral−derivative controllers and by recirculating heat-transfer oil held in a bath at T_{cryst}, which performs the cooling step with minimal undershoot (Figure 1). At the end of the crystallization process, the flow cell is withdrawn from the apparatus and quenched in cold water. The polymer sample is then extracted for ex situ microscopy.

Materials. There are three types of materials that we will describe in this paper. One is a typical Ziegler−Natta polypropylene with a broad distribution of molecular weight and stereoregularity; Ziegler−Natta materials have a polydispersity index, PDI = M_w/M_n, that is usually 6 or higher, in contrast to $M_w/M_n \approx 2-2.5$ that is typical for metallocene-derived polypropylenes, which also have uniform stereoregularity across all of the chains in the system. We will also examine the behavior of model metallocene materials and bidisperse systems comprised of these metallocene polymers in which a small concentration of very long chains is doped into a bulk material of much shorter chains.

The typical Ziegler−Natta polymer used for the experiments described here is a polydisperse isotactic polypropylene, PP-300/6 (weight-average molecular weight, $M_w \approx 300\,000$ g/mol; polydispersity index, PDI $\approx 6-8$; pentad content [mmmm] $\approx 96\%$; melt flow index = 12 dg/min at 230 °C under 2.16 kg load). The model polymers used have matched stereoregularity but very different mean chain lengths: "long" chains ($M_w \approx 825\,000$ g/mol; PDI ≈ 2.8) and "short" chains ($M_w \approx 180\,000$ g/mol; PDI ≈ 2.1). The isotactic pentad content of the "short" chains is [mmmm] = 95.4%, as determined by solution NMR. The "long" and "short" polymers have similar stereoregularity, as is evident from their IR spectra (ratio of bands at 998 and 973 cm^{-1}).

Flow-Induced Crystallization Experiments. The polymer was held at 225 °C for 5 min to erase its history (i.e., melt all the crystallites and relax previously developed stresses) before it was cooled to T_{cryst}. The structure that developed during and after shearing was followed using optical measurements with visible and X-ray radiation. Details of the optical[6,11] and X-ray[12] measurements have been described previously. Turbidity and birefringence measurements using visible 633 nm red light were made using an optical train consisting of a polarizer before the cell, aligned at 45° to the flow direction, and a polarizing beam splitter crossed with respect to the first polarizer, placed after the flow cell. Thus, the turbidity and birefringence are measured simultaneously. WAXD measurements were made at beamline X-27C at the National Synchrotron Light Source, Brookhaven National Laboratory. A liquid-cooled, 1024 × 1024 pixel CCD detector with a pixel resolution of 128.8 μm was used to acquire data. The WAXD data were calibrated using an α-alumina NIST standard. Ex situ TEM was performed either on stained thin sections or on replicas prepared as described previously.[12] Optical microscopy was performed on 5 μm sections cut from the quenched samples in the flow velocity gradient and the gradient−vorticity planes.

The calibration of the scale bars for the TEM micrographs were done using the grid spacing value specified by the manufacturer. We noticed a ±3% variation in the measured distance across the openings of the grid (well within the manufacturers ±10% specification). None of our conclusions is substantially affected by this 3% uncertainty.

Results and Discussion

Shear-Induced Kinetic Pathway to Nucleation. Our most significant (and surprising) result[13] is that, with *an increase in the temperature*, T_{cryst}, flow-induced oriented structures (whose birefringent signatures are observed in situ) *form at earlier times* (t_u) after flow inception (Figure 3), which is quite unexpected at temperatures far above the glass transition ($T_g \approx -5$ °C). The same wall shear stress, $\sigma_w = 0.06$ MPa, is imposed at all temperatures. Because the shear stress is directly related to the orientation distribution of polymer chain segments in the melt, imposition of the same level of stress effectively implies that, at a molecular level, the average orientation of the chains is held constant in all of the experiments. A comparison of the rheo-birefringence data with in situ WAXD and ex situ optical and electron microscopy confirms that these birefringent structures are indicative of the precursors that nucleate the formation of oriented crystals in the polydisperse Ziegler−Natta iPP (PP-300/6). The temperature dependence of the formation of these line nuclei during flow is especially striking when contrasted with the steep exponential increase in the crystallization time (t_Q) as T_{cryst} is increased in quiescent crystallization experiments (Figure 3), as is expected

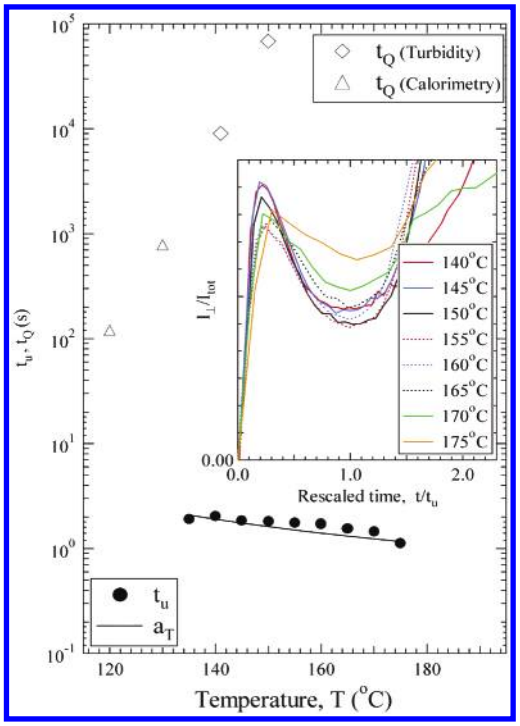

Figure 3. Temperature dependence of the time to form threadlike precursors in the polydisperse Ziegler−Natta iPP (PP-300/6) subjected to $\sigma_w = 0.06$ MPa, manifested in the upturn in the birefringence during shear. Inset: Birefringence traces plotted vs rescaled time using the temperature-dependent "upturn time", t_u. The magnitudes of the initial transient overshoot in $I_\perp/I_{tot}$ overlap to within 25% with the peak height decreasing with increasing temperature as expected for a melt undergoing inception of nonlinear shear under fixed stress. The subsequent upturn correlates with the appearance of oriented WAXD. The time for formation of these oriented crystallites (filled circles) is orders of magnitude faster than the quiescent crystallization time (open symbols) and has the opposite trend with temperature. The temperature dependence of the melt dynamics (a_T) is shown by the solid line. Reprinted with permission from ref 13. Copyright 2002 American Chemical Society.

based on classical nucleation theories. Interestingly, the decrease in the time for the formation of the line nuclei tracks the decrease in the melt relaxation time with increasing temperature (line in Figure 3).

Thus, under the influence of strong shear flow, the activation energy barrier that slows quiescent formation of nuclei with an increase in the temperature is virtually eliminated and line nuclei are formed via a nonclassical rheologically controlled pathway.[13] A number of nonclassical pathways to crystallization in polymers have been hypothesized such as nucleation of an intermediate phase (a rotator phase, a smectic phase, or a dense liquid phase) and activation of athermal nuclei. However, all of these mechanisms anticipate that the time for nucleation increases as the temperature increases, very unlike the temperature dependence that we discovered.

Threadlike Precursors Template Oriented Growth and Govern Impingement Time. For T_{cryst} below 170 °C, the upturn in the birefringent signal that indicates the formation of the threadlike nuclei during flow does not relax to zero even after cessation of flow[13] (Figure 4). Instead, it drops to a nonzero value as the sheared melt relaxes after flow cessation (the melt relaxation times at these temperatures are on the order of tens of milliseconds) and then increases as oriented crystallites develop. After flow cessation, crystallites

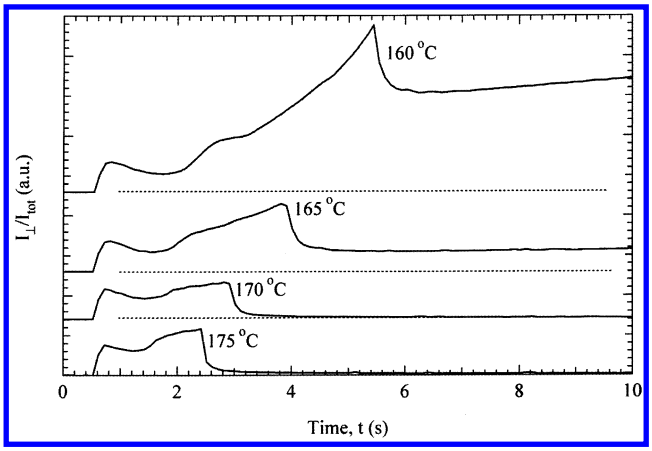

Figure 4. Transient birefringence during shear for PP-300/6 at $\sigma_w = 0.06$ MPa (as in Figure 3). Intensity transmitted through crossed polars $I_\perp/I_{tot}$ during and shortly after shear pulses. The formation of the usual overshoot during inception of nonlinear shear is evident at about 2 s. Later, at times where a melt would have reached its steady-state birefringence, there is a further upturn in the birefringence which does not relax to zero after cessation of flow. Reprinted with permission from ref 11. Copyright 2002 American Chemical Society.

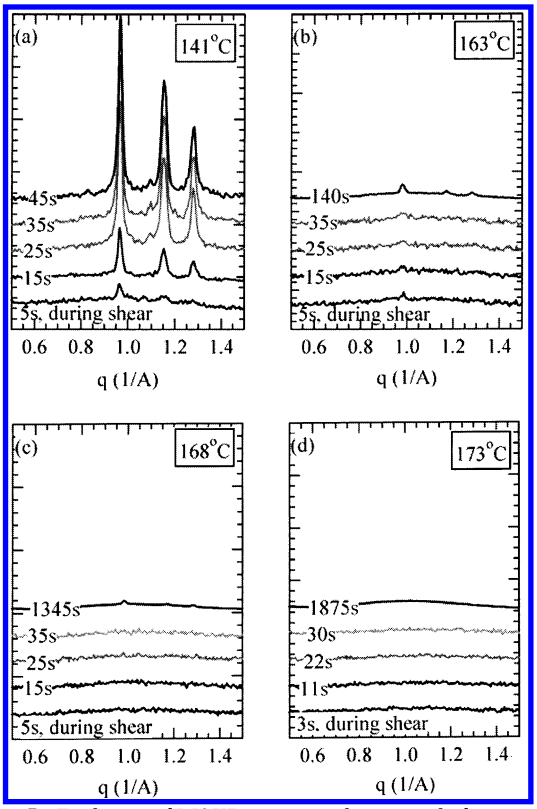

Figure 5. Evolution of WAXD intensity during and after cessation of shear for PP-300/6 at $\sigma_w = 0.06$ MPa at (a) 141 °C, (b) 163 °C, (c) 168 °C, and (d) 173 °C. These one-dimensional traces show a slice of the two-dimensional WAXD pattern perpendicular to the flow direction (see Figure 6) and have been normalized for acquisition time at each temperature. Reprinted with permission from ref 13. Copyright 2002 American Chemical Society.

grow out radially from the line nuclei, advancing at their quiescent growth velocity, which decreases strongly with increasing temperature. Thus, the increase in the WAXD intensities after flow cessation slows with an increase in T_{cryst} and drops to zero at the nominal melting point, $T_{nom} \approx 170$ °C (Figure 5). The rate at which a comparable WAXD intensity is achieved after shearing at different T_{cryst} matches well with literature

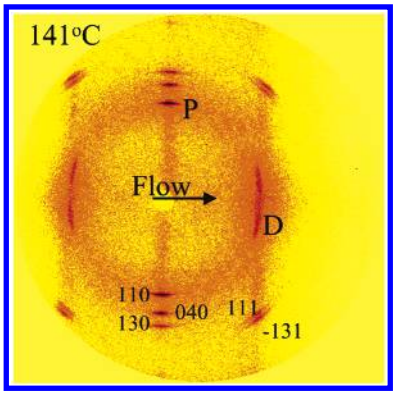

Figure 6. Two-dimensional WAXD pattern during shear at 141 °C for PP-300/6 at $\sigma_w = 0.06$ MPa. The diffracting planes are as indicated. "Parent" crystallites (P) are observed with the chain (*c*) axis oriented along the flow direction. These are accompanied by epitaxial "daughter" (D) crystallites oriented at approximately ±80° with respect to the parents.

values of the linear crystal growth velocities at those temperatures. Thus, while the birefringent signature indicating formation of the oriented nucleation precursor is observed even above $T_{nom} \approx 170$ °C, crystallites only grow laterally from these precursors if T_{cryst} is below 170 °C, where crystal growth velocities are nonzero.

Two-dimensional WAXD patterns obtained as the crystallites form, *during flow* ($T_{cryst} = 141$ °C, $\sigma_w = 0.06$ MPa, and $t_s = 12$ s), confirm that the monoclinic α-phase crystals that are formed are strongly oriented with the polymer chain (*c*) axis along the flow direction[12] (Figure 6). The intensity of the crystalline reflections as a function of scattering vector (circular average of the two-dimensional WAXD image over the azimuthal angle, $f = 0-2\pi$ rad) can be used to estimate the extent of crystallinity. The WAXD peak intensity grows rapidly (Figure 7a) for the first 100 s (just 1% of t_Q), after which

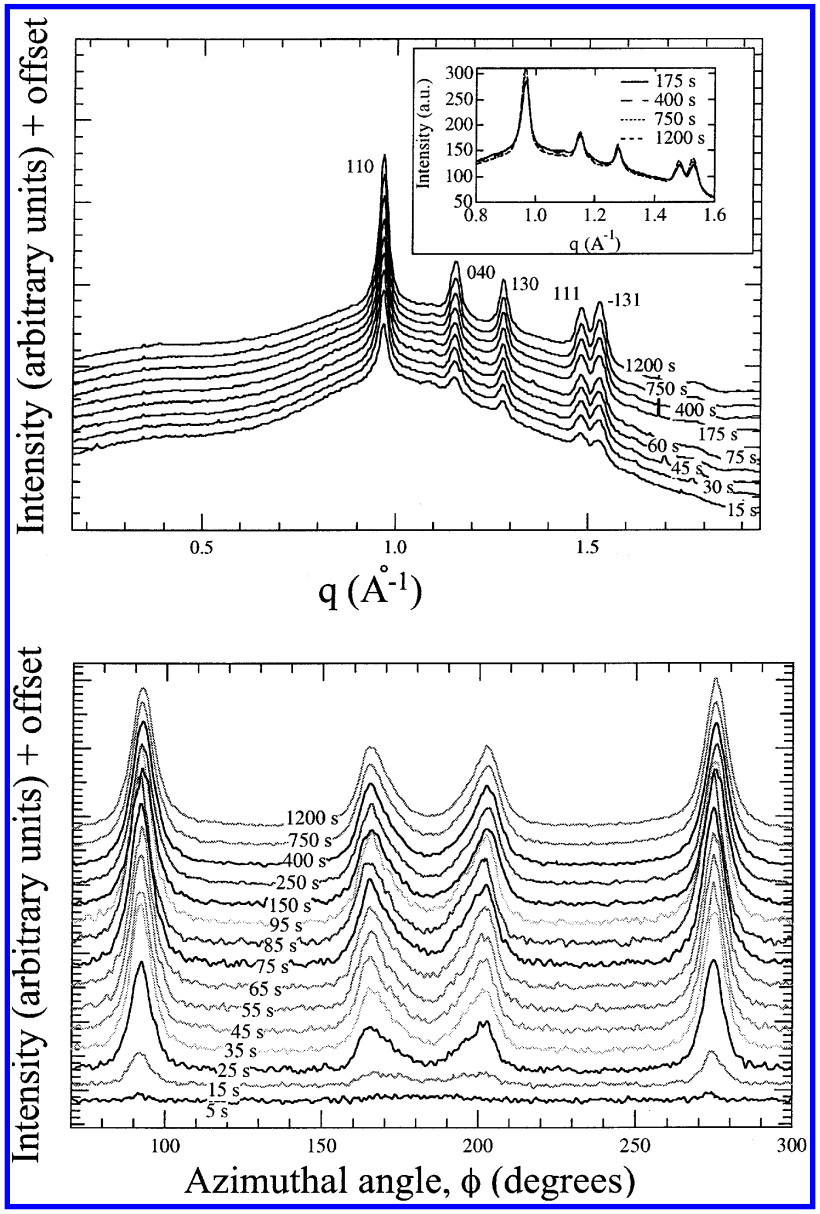

Figure 7. Development and orientation of crystallinity as a function of crystallization time for PP-300/6 after the imposition of shear ($\sigma_w = 0.06$ MPa and $t_s = 12$ s at 141 °C). Top: Evolution of the circularly averaged powder WAXD patterns, normalized for data acquisition time. The data are vertically offset for clarity. The inset shows scans at $t_{cryst} = 175$, 400, 750, and 1200 s without an offset. Bottom: Evolution of the azimuthal profile of intensity at the [110] crystalline peak showing that the orientation distribution of crystallites remains sharp as growth proceeds. The data are scaled for acquisition time and vertically offset for clarity. Reprinted with permission from ref 12. Copyright 2000 Elsevier Science.

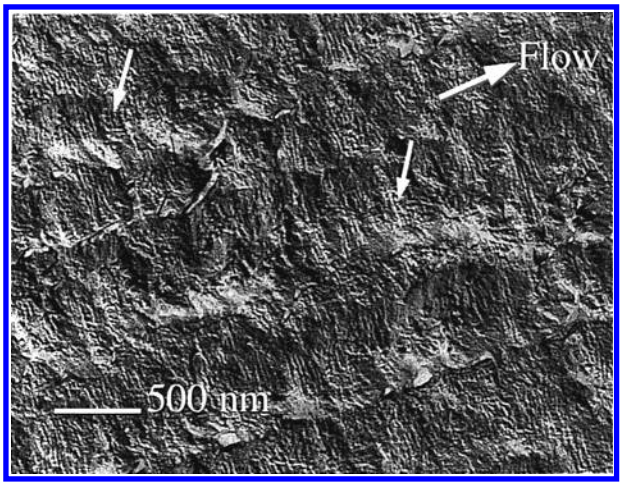

Figure 8. TEM micrograph of the row-nucleated structure approximately 40 μm from the wall of the shear cell, near the transition to unoriented structures, showing details of the lamellar structure in the oriented skin. The primary lamellae are perpendicular to the flow direction. The interline spacing is approximately 700 nm. Two of the regions where cross-hatching is apparent are indicated with arrows. Reprinted with permission from ref 12. Copyright 2000 Elsevier Science.

the WAXD crystallinity "saturates", growing only very slowly over the next 1000 s (Figure 7a, inset). Electron micrographs of the final structure show that the oriented "skin" has a row-nucleated morphology with row spacing from 250 to 750 nm. The small distance between the threadlike precursors explains the rapid completion of the oriented skin. The saturation in the WAXD data, taken together with the TEM, indicates that crystals grow out radially from the line nuclei until they impinge, at which time the rate of the increase in crystallinity slows down tremendously.

Time-resolved azimuthal scans at a scattering vector corresponding to the [110] peak indicate that the WAXD arcs remain narrow as the sample crystallizes (Figure 7b). Thus, the oriented line nuclei that are generated during the brief interval of shear template the orientation distribution of crystallites that grow laterally from them.[12] Therefore, theoretical models of the formation of threadlike precursors are required to accurately predict the kinetics and morphology of crystallization.

The α-phase of iPP is known to demonstrate a unique epitaxial behavior where "daughter" lamellae are nucleated on existing parent crystals with the *a* and *c* axes of one crystal parallel to the *c* and *a* axes of the other. This spontaneous cross-reinforcement is responsible for some of the desirable properties of polypropylene, sometimes called "the living hinge". For oriented crystals, this crystallographic branching leads to parent *and* daughter WAXD [110] arcs; thus, the azimuthal scan shows four daughter peaks in addition to the two parent peaks. Interestingly, daughter peaks form at almost the same time as the parent peaks and are apparent even during shearing (Figures 6 and 7b). These daughter lamellae are clearly visible in ex situ TEM images and are observed to grow with their chain direction nearly perpendicular to the flow direction (Figure 8).

Threadlike Precursors: Elongation and Saturation. We now turn to an examination of the manner in which the oriented nuclei that are formed during the initial brief shearing develop into the final cylindrulites that are observed in TEM images of the skin. First, we present in situ rheo-optical data that provide a macroscopic picture of the effect of shear stress, σ_w, and shearing duration, t_s, on crystal development. Then, we present ex situ optical and TEM micrographs that show the crystalline structure that develops for different t_s at high σ_w. The microstructure observed ex situ at the end of the crystallization experiment is used to infer the structure that forms during flow and the nature of growth from the flow nuclei.

At 141 °C, the quiescent crystallization "half-time", $t_{1/2}$, viz., the time taken for the sample in the flow cell to become turbid, is approximately 10^4 s (Figure 9). Applications of brief intervals of shear, ranging from 0.25 to 12 s at $\sigma_w = 0.06$ MPa and up to 16 s at $\sigma_w = 0.03$ MPa, progressively reduce the time for the material to become turbid, a signature of the appearance of crystallites (Figure 9). Thus, shear crystallization experiments both at $\sigma_w = 0.03$ MPa and at $\sigma_w = 0.06$ MPa show a reduction in $t_{1/2}$ by about 2 orders of magnitude. However, the crystallites formed at these two σ_w have a very different superstructure. At the lower σ_w (=0.03 MPa), no birefringent upturn is observed during shear (Figure 9a, inset) even at the longest t_s. Correspondingly, the strongly anisotropic "skin−core" morphology typical of strongly sheared samples is not observed in ex situ polarizing optical micrographs. As σ_w is increased to 0.06 MPa, we can observe the transition to oriented growth as a function of the shearing duration. For shearing times up to approximately 4 s, there is no optical signature of highly oriented growth: neither is there an upturn in the birefringence during shear nor does the optical anisotropy increase substantially as the crystallites grow after shearing. However, for longer shearing times, there is a significant upturn in the birefringence during shear and the optical anisotropy after flow cessation grows strongly—a signature that the crystallites are growing with a preferred orientation. When the samples are removed for observation of the morphology as a function of depth, this change in orientational behavior inferred from the birefringence observed in real time correlates with the change in morphology. The samples that showed little birefringence in situ also lacked a highly oriented skin when sectioned and observed through cross-polarizers.

Our in situ rheo-turbidity and birefringence studies confirm some of the features of the phenomenological picture put forward by Janeschitz-Kriegl[10] to describe microstructural evolution. According to his model, the cascade of events begins with the formation of pointlike precursors during shear; subsequently, threadlike precursors propagate from these pointlike precursors during the continued shearing, and oriented crystals grow radially from the threads or line nuclei. However, while their model predicts a monotonic dependence of crystallization time on shearing duration, our turbidity data show saturation beyond $t_s \approx 4$ s.

To obtain a clearer picture of how the line nuclei develop with increasing t_s, we observe the morphology of samples sheared isothermally for $t_s = 1$, 2, 4, and 8 s and grown to impingement prior to removal. For $t_s = 1$ s, there is a much higher nucleation density near the wall than in the core of the sample (Figure 10a, optical micrograph). On the time scale of this experiment, negligible quiescent nucleation occurs, evidenced by the absence of nuclei between 100 μm depth from the wall and the center of the sample (i.e., all of the nuclei observed are activated by flow). There is a strongly nonlinear dependence of the nucleation density with distance from the wall, indicating the nonlinear effect

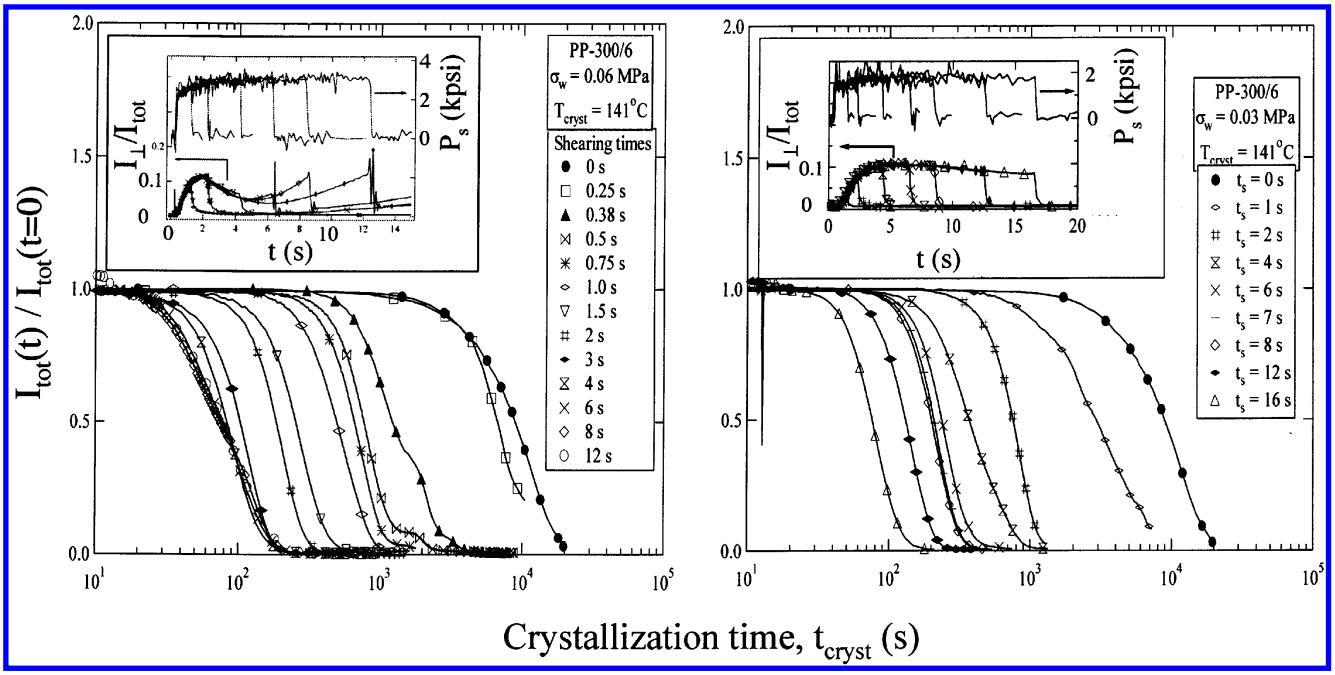

Figure 9. Effect of shearing time on crystallization kinetics of PP-300/6 manifested in the turbidity following a "pulse" of shear at 141 °C: (a) $\sigma_w = 0.06$ MPa; (b) $\sigma_w = 0.03$ MPa. The curves show the experimental data; symbols are sparsely distributed on the lines to distinguish experiments with different shearing times. Scattering of incident light as the polymer crystallizes decreases the transmitted intensity. The time at which the transmitted intensity is reduced by half, $t_{1/2}$, decreases with increasing shearing time; for stress large enough to induce the formation of threadlike precursors (a), $t_{1/2}$ reaches a plateau after a shearing time of about 4 s.

of shear stress (which increases linearly from the center to the wall).

When the microstructure of the sample sheared for 2 s is compared to the one sheared for 1 s (Figure 10b vs Figure 10a), it is evident that long (several microns) threadlike precursors developed between 1 and 2 s during shear.[16] The result is an oriented skin that shows light striations when viewed at 45° through crossed polarizers and appears black when the flow direction is aligned along the polarizer or analyzer (in contrast to the spherulitic structure at depths greater than ~60 μm, which show bright portions consistently as the sample is rotated between crossed polars). WAXD results reveal that the low birefringence of the skin for $t_s = 2$ s results from the relatively high ratio of daughter to parent crystallites. If shear is continued for an additional 2 s, there is a further proliferation of threadlike precursors, seen in the much smaller spacing between threadlike precursors in the $t_s = 4$ s sample and the much greater birefringence of the oriented skin.

The morphology hardly changes as the shearing is sustained for $t_s = 8$ s. The thickness of the oriented skin is essentially constant across samples sheared for 2, 4, or 8 s. This result is interesting because it suggests that there is a threshold stress below which the formation of threadlike precursors is simply not triggered by the shear flow and that shearing for a longer duration does not enable the formation of threads at greater depth or correspondingly lower shear stresses. Moreover, another sort of saturation is also evident in the images, and that is in the density of threads. The average spacing between the threads that is observed for $t_s = 4$ s is not substantially changed when the shear is sustained for 8 s (Figure 10c,d). This explains the saturation behavior in the turbidity shown earlier, in which the time trace of the transmitted intensity is virtually indistinguishable for samples that were sheared for 4, 6, 8, or 12 s.

The ex situ microscopy results show that the oriented X-ray and birefringence signals observed in real time in situ arise from the outermost 60−70 μm of the sample. The window of shearing time that produces a strong nonlinear decrease in the turbidity halftime correlates with the time during which the pointlike nuclei form and threads (or line nuclei) begin to grow and lengthen. Once the shearing duration is long enough to generate a saturated density of threads, the time course of the transient turbidity after cessation of shear saturates as well.

Role of Long Chains in the Formation of Threadlike Precursors. Our experiments with the polydisperse resin point to a rheological route to crystal nucleation in sheared polymer melts; however, it is difficult to infer the molecular variables that govern this process for such an ill-defined resin. The typical Ziegler−Natta catalysts are heterogeneous and contain a multiplicity of active sites for polymerization. The iPPs they produce are not only polydisperse with respect to molecular mass distribution (with polydispersity indices typically higher than 4); the stereoregularity of the chains is correlated with the chain length—high molecular weight chains tend to be more stereoregular.[18] Recent advances in "single-site" metallocene catalysts offer the possibility of understanding the role of both types of polydispersity in governing the processing−morphology−property relations of iPP. Thus, we have recently started examining well-defined metallocene iPPs, with relatively narrow molecular mass distribution and uniform levels of tacticity across all of the molecules.[13,14]

To isolate the role of molecular weight distribution from that of the average molecular weight, we studied the effect of shear on the crystallization of two model resins with very different molecular weights (186 kg/mol "short" and 825 kg/mol "long") but similar relatively narrow polydispersity ($M_w/M_n \approx 2-3$) and matched stereoregularity ([mmmm] ≈ 96%). Molecular mass polydispersity was introduced in a controlled manner by carefully blending a small weight fraction of the long

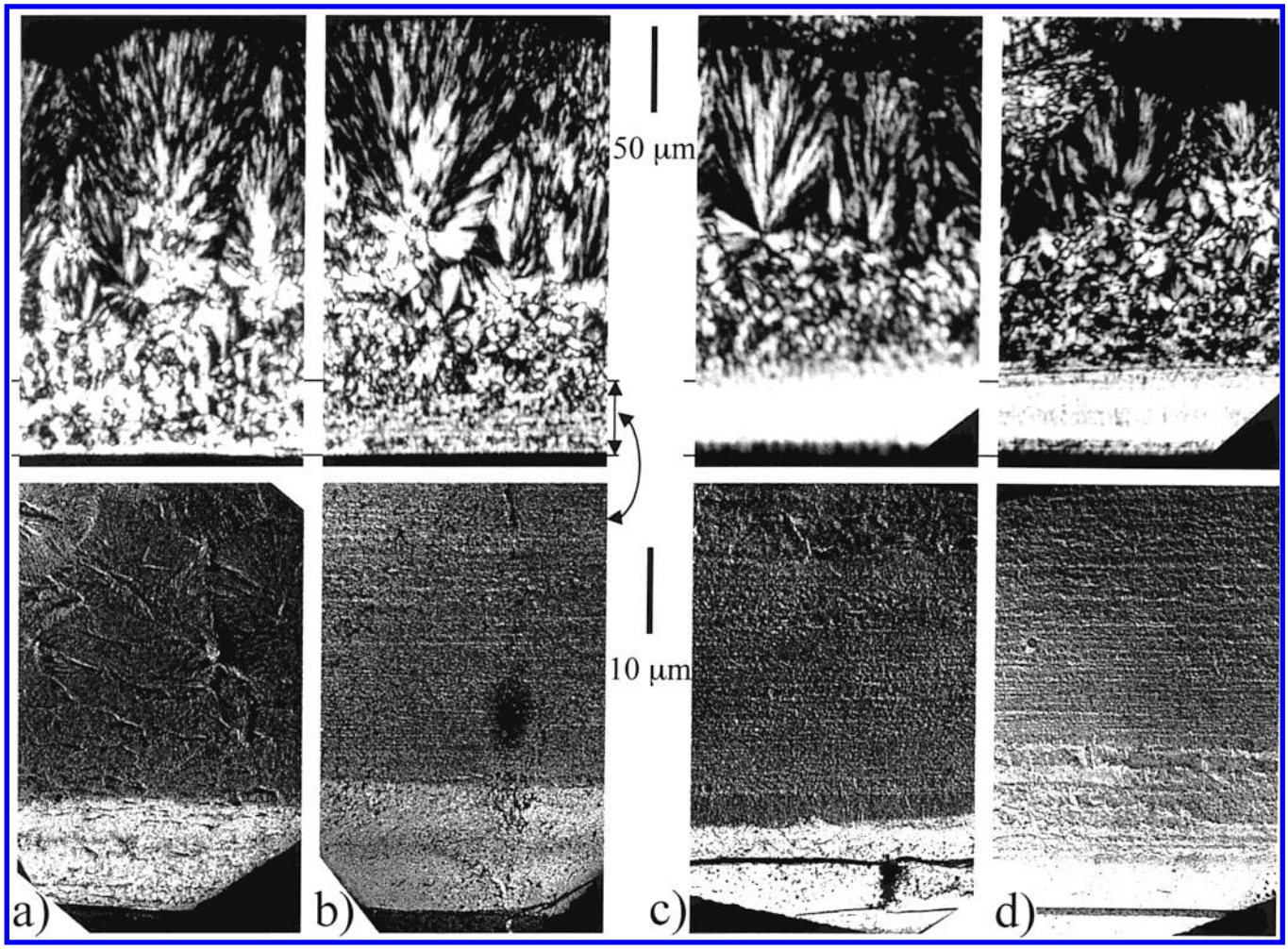

Figure 10. Polarized light micrographs (top) and electron micrographs (bottom) of the final solid-state morphology of PP-300/6 subjected to short-term shearing with $\sigma_w = 0.06$ MPa at $T = 141$ °C for shearing times (a) $t_s = 1$ s, (b) 2 s, (c) 4 s, and (d) 8 s. Images in polarized light are sections in the (v, ∇v) plane viewed through crossed polarizers, as indicated in Figure 11. During t_s the shear stress is a maximum at the walls, decreasing linearly to zero at the center of the sample. The effect of increasing shearing time on the large-scale morphology (top) shows the formation and thickness of the oriented skin, as well as the development of pointlike nuclei in the fine-grained region between the skin and the core. The detailed morphology near the surface (bottom) shows that threadlike precursors form between 1 and 2 s during shear, increase in concentration between 2 and 4 s during shear, but do not change appreciably between 4 and 8 s during shear.

chains into the short chains. Shearing the polymer at a high σ_w, sufficient to induce oriented "skin−core" morphologies in the polydisperse Ziegler−Natta material, led to accelerated crystallization rates in the pure long and short materials; however, an oriented crystalline skin was not formed in the individual components. In contrast, the transition to oriented growth occurred readily upon shearing the bidisperse blends (Figure 11).

Only a small weight fraction of the long component was added to the blend, so its rheology was not significantly different from that of the pure short component; hence, almost all measures of the imposed flow were held constant in the comparison between the pure short polymer and the binary blends (the shear stress, shearing time, and total imposed strain are all approximately the same). Because the level of stress used in all of the experiments with the model materials is kept constant, the *average* deformation experienced by the polymer chains is identical. However, while all the polymers in the monomodal materials experience roughly the same chain deformation, in the bidisperse materials, the long, slow-relaxing chains are preferentially deformed as compared to the short chains. Thus, it appears that the high levels of chain distortion experienced by the slow-relaxing species in resins with a broad distribution of relaxation times greatly promotes the generation of oriented nuclei.

On a molecular level, this raises questions about how the long chains exert their effect. We began by addressing the following question: is the mechanism of the long-chain effect a single-chain process or a cooperative one? Therefore, we examined the effect of the concentration of the long chains on the development of orientation to see if the dependence was linear (consistent with a single-chain effect) or nonlinear (suggesting a cooperative effect). The results show a distinctly nonlinear, sigmoidal-type concentration dependence: weak enhancement of thread formation at concentrations below the long chain−long chain overlap concentration c^*, strong enhancement of thread formation as the long-chain concentration reaches c^*, and weak effects of further addition of long chains.[14] This importance of long chain−long chain overlap suggests that the formation of the oriented nucleation precursors is a cooperative effect, involving more than a single long chain. Further model materials are required to determine how the effect of the long chains depends on their relative relaxation time compared to the short-chain matrix and

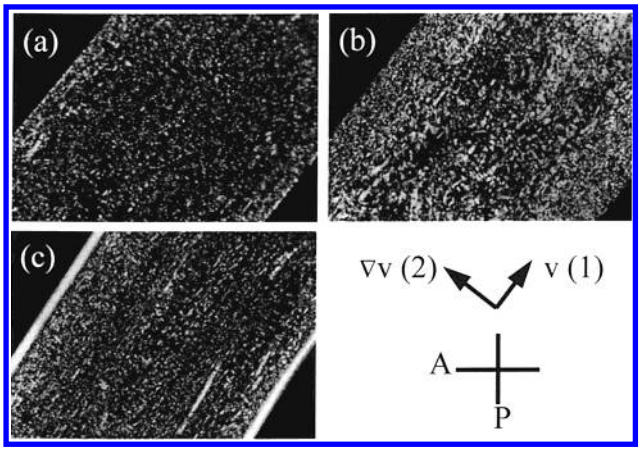

Figure 11. Polarized light micrographs of the final solid-state morphology of model isotactic polypropylenes subjected to short-term shearing with $\sigma_w = 0.06$ MPa at $T = 142$ °C viewed through crossed polarizers (oriented as indicated). Samples "short" and "long" are described in the text. (a) "Short" iPP sheared for $t_s = 2.2$ s, (b) "long" iPP sheared for $t_s = 300$ s, and (c) a binary blend of 2% long and 98% short sheared for $t_s = 2.25$ s. Only the binary blend shows the shear-induced formation of oriented precursors manifested by the highly oriented skin (bright when viewed through crossed polarizers). Reprinted with permission from ref 13. Copyright 2002 American Chemical Society.

on their relative stereoregularity compared to the short chains. This knowledge could guide the selection of combinations of single-site catalysts to directly synthesize desired distributions of molecular weight and stereochemistry. A deeper molecular level understanding can guide a new generation of theoretical models that relate melt dynamics during processing to the development of crystallization precursors and predict the morphology and kinetics of growth templated by these precursors.

Conclusions

Our work provides tantalizing glimpses of the molecular processes that underlie the formation of crystalline microstructure as a polymer melt crystallizes after shearing. Novel instrumentation allows us to apply the "short-term shearing" protocol with multiple structural probes and enables studies of model materials available in small quantities. Shearing the polymer at a high wall shear stress, above the value at which we see oriented crystal growth, leads to the development of threadlike nucleation precursors that are identified in real time via their birefringent and WAXD signatures and ex situ by their morphological fingerprint seen in electron micrographs of the final solid state. These precursors form even above the nominal melting point, T_{nom}, for the polymer. The timescale for formation of the threadlike precursors as a function of temperature tracks the rate of molecular motion, a behavior that is unanticipated at $T \gg T_g$. Below T_{nom}, the precursors act as highly effective nuclei for crystallization and template the growth of monoclinic α crystals that grow radially from them at the quiescent growth velocity until they "impinge". Ex situ electron microscopy on samples crystallized after shearing for different durations indicates that the nuclei form during shear and then extend along the flow direction as shear is continued, until the microstructure saturates. Model polymers with a bimodal molecular weight distribution show that (1) the mechanism of formation of the threadlike precursors preferentially involves the longest chains in the melt, (2) chains 4.7 times longer than average are "long enough" to enhance the formation of threadlike precursors, and (3) the long chains act cooperatively, benefitting greatly from long chain−long chain overlap.

Acknowledgment

We are very grateful to Dr. A. Prasad (Equistar Chemical) and Dr. R. L. Sammler (The Dow Chemical Co.) for providing the materials used in our studies. Synchrotron experiments were carried out at the beamline X27C of the National Synchrotron Light Source, Brookhaven National Laboratory, which is supported by the U.S. Department of Energy, Divisions of Material Sciences and Chemical Sciences, under Contract DE-AC02-98CH10886. This work was made possible by a number of funding sources: Financial support from Proctor and Gamble, the Cargill-NIST ATP, the Schlinger fund, and NSF (DMR9901403 and PHY99-07949) is gratefully acknowledged.

Literature Cited

(1) Kaplan, W. A., Ed. *Modern Plastics Encyclopedia*; McGraw-Hill: New York, 1998.

(2) van Krevelen, D. Crystallinity of Polymers and the Means to Influence the Crystallization Process. *Chimia* **1978**, *32*, 279. Meijer, H., Ed. *Processing of Polymers*; VCH: New York, 1997; Vol. 18.

(3) Bassett, D. *Principles of Polymer Morphology*; Cambridge University Press: Cambridge, U.K., 1981.

(4) Doi, M.; Edwards, S. F. *The Theory of Polymer Dynamics*; Oxford Publications: Oxford, U.K., 1986. Larson, R. G. *Constitutive Equations for Polymer Melts and Solutions*; Butterworth: New York, 1988.

(5) Pearson, J. R. A. *Mechanics of Polymer Processing*; Elsevier: New York, 1985.

(6) Kumaraswamy, G.; Verma, R. K.; Kornfield, J. A. Novel Flow Apparatus for Investigating Shear-Enhanced Crystallization and Structure Development in Semicrystalline Polymers. *Rev. Sci. Instrum.* **1999**, *70*, 2097 and references therein.

(7) Peterlin, A. Drawing and Extrusion of Semicrystalline Polymers. *Colloid Polym. Sci.* **1987**, *265*, 357.

(8) Mencik, Z.; Fitchmun, D. R. Texture of Injection Molded Polypropylene. *J. Polym. Sci., Polym. Phys.* **1973**, *11*, 973. Fitchmun, D. R.; Mencik, Z. Morphology of Injection Molded Polypropylene. *J. Polym. Sci., Polym. Phys.* **1973**, *11*, 951. Fujiyama, M.; Wakino, T.; Kawasaki, Y. Structure of Skin Layer in Injection Molded Polypropylene. *J. Appl. Polym. Sci.* **1988**, *35*, 29. Fujiyama, M.; Wakino, T. Distribution of Higher Order Structures in Injection Molded Polypropylenes. *J. Appl. Polym. Sci.* **1991**, *43*, 57. Isayev, A. I.; Chan, T. W.; Shimojo, K.; Gmerek, M. Injection Molding of Semicrystalline Polymers. I. Material Characterization. *J. Appl. Polym. Sci.* **1995**, *55*, 807. Lopez, L.; Cieslinski, R.; Putzig, C.; Wesson, R. Morphological characterization of injection moulded syndiotactic polystyrene. *Polymer* **1995**, *36*, 2331. Ulcer, Y.; Cakmak, M.; Miao, J.; Hsiung, C. Structural Gradients Developed in Injection-Molded Syndiotactic Polystyrene (sPS). *J. Appl. Polym. Sci.* **1996**, *60*, 669. Ulcer, Y.; Cakmak, M. Texture of injection molded poly(ethylene-2,6-naphthalene dicarboxylate) parts. *Polymer* **1997**, *38*, 2907. Dees, J. R.; Spruiell, J. E. Structure development During Melt Spinning of Linear Polyethylene Fibers. *J. Appl. Polym. Sci.* **1974**, *18*, 1053. Gupta, R. K.; Auyeung, K. F. Crystallization Kinetics of Oriented Polymers. *Polym. Eng. Sci.* **1989**, *29*, 1147. Misra, S.; Lu, F. M.; Spruiell, J. E.; Richeson, G. C. Influence of Molecular Weight Distribution on the Structure and Properties of Melt Spun Polypropylene Filaments. *J. Appl. Polym. Sci.* **1996**, *56*, 1761. McHugh, A.; Guy, R.; Tree, D. Extensional flow-induced crystallization of a polyethylene melt. *Colloid Polym. Sci.* **1993**, *271*, 629.

(9) Haas, T.; Maxwell, B. Effects of Shear on the Crystallization of Linear Polyethylene and Polybutene−1. *Polym. Eng. Sci.* **1969**, *9*, 225. Kobayashi, K.; Nagasawa, T. Crystallization of sheared polymer melts. *J. Macromol. Sci., Phys.* **1970**, *B4*, 331. Wereta, A., Jr.; Gogos, C. Crystallization Studies on Deformed Polybutene−1. Melts. *Polym. Eng. Sci.* **1971**, *11*, 19. Lagasse, R.; Maxwell, B.

An Experimental Study of the Kinetics of Polymer Crystallization During Shear Flow. *Polym. Eng. Sci.* **1976**, *16*, 189. Andersen, P.; Carr, S. Flow-Induced Crystallization of Polypropylene in Stretched Ribbons. *Polym. Eng. Sci.* **1976**, *16*, 217. Andersen, P.; Carr, S. Crystal Nucleation in Sheared Polymer Melts. *Polym. Eng. Sci.* **1978**, *18*, 215. Ulrich, R.; Price, F. Morphology Development During Shearing of Poly(ethylene Oxide) Melts. *J. Appl. Polym. Sci.* **1976**, *20*, 1077. Sherwood, C.; Price, F.; Stein, R. Effect of Shear on the Crystallization Kinetics of Poly(ethylene Oxide) and Poly(ϵ-Caprolactone) Melts. *J. Polym. Sci., Polym. Symp.* **1978**, *63*, 77. Wolkowicz, M. Nucleation and Crystal Growth in Sheared Poly(1-Butene) Melts. *J. Polym. Sci., Polym. Symp.* **1978**, *63*, 365. Tribout, C.; Monasse, B.; Haudin, J. Experimental study of shear-induced crystallization of an impact polypropylene copolymer. *Colloid Polym. Sci.* **1996**, *274*, 197. Vleeshouwers, S.; Meijer, H. A rheological study of shear induced crystallization. *Rheol. Acta* **1996**, *35*, 391. Duplay, C.; Monasse, B.; Haudin, J. M.; Costa, J. L. Shear-induced Crystallization of Polypropylene: Influence of Molecular Structure. *J. Mater. Sci.* **2000**, 35. Floudas, G.; Hilliou, L.; Lellinger, D.; Alig, I. Shear-Induced Crystallization of Poly(ϵ-Caprolactone). 2. Evolution of Birefringence and Dichroism. *Macromolecules* **2000**, *33*, 6466.

(10) Janeschitz-Kriegl, H.; Eder, G. Basic concepts of structure formation during processing of thermoplastic materials. *J. Macromol. Sci., Chem.* **1990**, *A27* (13 & 14), 1733. Eder, G.; Janeschitz-Kriegl, H.; Liedauer, S. Crystallization processes in quiescent and moving polymer melts under heat transfer conditions. *Prog. Polym. Sci.* **1990**, *15*, 629. Eder, G.; Janeschitz-Kriegl, H. Crystallization. *Mater. Sci. Technol.* **1997**, *18*, 268. Liedauer, S.; Eder, G.; Janeschitz-Kriegl, H.; Jerschow, P.; Geymayer, W.; Ingolic, E. On the Kinetics of Shear Induced Crystallization in Polypropylene. *Int. Polym. Proc.* **1993**, *8*, 236. Jerschow, P.; Janeschitz-Kriegl, H. The Role of Long Molecules and Nucleating Agents in Shear Induced Crystallization of Isotactic Polypropylenes. *Int. Polym. Proc.* **1997**, *12*, 72. Liedauer, S.; Eder, G.; Janeschitz-Kriegl, H. On the Limitation of Shear Induced Crystallization in Polypropylene Melts. *Int. Polym. Proc.* **1995**, *10*, 243.

(11) Kumaraswamy, G.; Issaian, A. M.; Kornfield, J. A. Shear-Enhanced Crystallization in isotactic Polypropylene. 1. Correspondence between In-situ Rheo-Optics and Ex-situ Structure Determination. *Macromolecules* **1999**, *32*, 7537.

(12) Kumaraswamy, G.; Verma, R. K.; Issaian, A. M.; Wang, P.; Kornfield, J. A.; Yeh, F.; Hsiao, B. S.; Olley, R. H. Shear-Enhanced Crystallization in isotactic Polypropylene. 2. Analysis of the formation of the oriented skin. *Polymer* **2000**, *41*, 8931.

(13) Kumaraswamy, G.; Kornfield, J. A.; Yeh, F.; Hsiao, B. S. Shear-Enhanced Crystallization in isotactic Polypropylene. 3. Evidence for a Kinetic Pathway to Nucleation. *Macromolecules* **2002**, *35*, 1762.

(14) Seki, M.; Thurman, D.; Oberhauser, J.; Kornfield, J. A. Shear-mediated Crystallization of isotactic Polypropylene. The Role of Long Chain-Long Chain Overlap. *Macromolecules* **2002**, *35*, 2583.

(15) Macosko, C. W. *Rheology: principles, measurements and applications*; VCH: New York, 1993.

(16) Recently, Petermann and co-workers have presented evidence that threadlike precursors can propogate into a quiescent melt.[17] They suggest that such propogation results from an "autocatalytic" extension at the ends of a shish due to polymer chains being reeled in and stretched as they come into registry with the shish. According to them, such an extension is suppressed when the polymer shows a stronger tendency to form chain-folded crystals rather than stretching and lining up with the shish. In our experiments on highly isotactic iPP, in situ WAXD and SAXS indicate that chain-folded lamellae (and even epitaxial daughter crystals) form on very shoft time scales, during shear. This suggests that shish extension after cessation of flow via the mechanism proposed by Petermann and co-workers would not contribute significantly to the overall length of the shish. Further, Petermann shows a shish extension of less than a micron for a low tacticity isotactic polystyrene, while in our highly isotactic iPP (with a higher tendency toward chain folding), the shear-induced extension of the shish from $t_s = 1$ to 2 s is tens of microns. Finally, if we assume that the factors that control shish extension remain the same as the shearing time is increased from 1 to 2 s or more, the needles observed in the micrographs for $t_s = 1$ s provide an upper bound for the amount of propagation following cessation of flow. This is substantially shorter than the shish lengths observed for shearing times equal to or exceeding 2 s. Thus, we feel that it is very unlikely that the shish observed in our experiments elongate significantly (if at all) subsequent to flow cessation.

(17) Lieberwirth, I.; Loos, J.; Petermann, J.; Keller, A. Observation of Shish Crystal Growth into Nondeformed Melts. *J. Polym. Sci., Polym. Phys.* **2000**, *38*, 1183.

(18) Paukkeri, R.; Iiskola, E.; Lehtinen, A.; Salminen, H. Microstructural Analysis of Polypropylenes polymerized with Ziegler−Natta Catalysts without External Donors. *Polymer* **1995**, *36*, 3969. Paukkeri, R.; Vaananen, T.; Lehtinen, A. Microstructural Analysis of Polypropylenes produced with heterogeneous Ziegler−Natta Catalysts. *Polymer* **1993**, *34*, 2488.

Received for review April 1, 2002
Revised manuscript received May 24, 2002
Accepted June 6, 2002

IE020237Z